Applied Catalysis B: Environmental 219 (2017) 30–35

Contents lists available at ScienceDirect

Applied Catalysis B: Environmental

journal homepage: www.elsevier.com/locate/apcatb

Designing of a spatially separated hetero-junction pseudobrookite (Fe_2TiO_5-TiO_2) yolk-shell hollow spheres as efficient photocatalyst for water oxidation reaction

Muhammad Waqas[a,b,1], Shahid Iqbal[c,1], Ali Bahadur[d,*], Aamer Saeed[d], Muhammad Raheel[e], Mohsin Javed[f]

[a] State Key Laboratory of Biochemical Engineering, CAS Center for Excellence in Nanoscience, Institute of Process Engineering, Chinese Academy of Sciences, 1 North 2nd Street, Zhongguancun, Haidian District, Beijing 100190, PR China
[b] University of the Chinese Academy of Sciences, Chinese Academy of Sciences, No. 19A Yuquanlu, Beijing 100049, PR China
[c] School of Chemistry and Chemical Engineering, University of Chinese Academy of Sciences, Beijing 100049, PR China
[d] Department of Chemistry, Quaid-i-Azam University, Islamabad 45320, Pakistan
[e] Department of Chemistry, Balochistan University of Information Technology, Engineering and Management Sciences, Quetta, Pakistan
[f] Department of Chemistry, School of Science, University of Management and Technology, C-II, Johar Town, Lahore, Pakistan

ARTICLE INFO

Article history:
Received 10 June 2017
Received in revised form 15 July 2017
Accepted 17 July 2017
Available online 19 July 2017

Keywords:
Yolk-shell hollow spheres
Titanium oxide
Pseudobrookite
Hetero-junction photocatalytic water oxidation

ABSTRACT

For the first time, controlled pseudobrookite phase as the yolk and titanium oxide as the shell of hollow spheres were synthesized for the photocatalytic water oxidation. Simple and facile sacrificial hard template strategy was utilized. Firstly, the distribution of TiO_2 in the hollow spheres was controlled by loading aqueous solution of 2, 3, and 5 mol/L $TiCl_4$ precursor respectively onto carbonaceous template followed by annealing. To prove the Fe^{3+} ions radial penetration into the hydrophobic core of carbonaceous template, we optimized the ethanol to water ratio. The Fe_2TiO_5-TiO_2 yolk-shell hollow spheres exhibited high oxygen evolution reaction (OER) rate up to 148 $\mu mol\ g^{-1}\ h^{-1}$ under UV–vis light. This was attributed to the better light harvesting due to the geometry of hollow sphere; charge separation by a thin shell-yolk hetero-junction, a void cavity to access reaction solvent to reactive sites and the hetero-junction of Fe-O-Ti in the hollow structure. These findings suggest that our designed Fe_2TiO_5-TiO_2 yolk-shell hollow spheres are beneficial for the photocatalytic water oxidation.

1. Introduction

Carbon dioxide emission affects the global climate, which is a serious threat to living beings. To develop a catalyst by utilizing low cast abundant materials and synthetic methodology is a vital step towards sustainable energy [1]. For its simplicity, the semiconductor powdered catalyst in the suspension is the potential candidate in the water splitting reactions. The working principle for water splitting involved several microscopic steps. Firstly, exciton generation upon light absorptions, [2] secondly, charge separation and finally suitable band edge positions; valence band (VB) and conduction band (CB) straddle the redox potentials of target reactions [3,4].

TiO_2 and Fe_2O_3 fulfill the several principles requirements for solar water splitting and are reported frequently in the literature [5,6]. Demerits of TiO_2 are; large band gap (~3.2 eV), which constitute only 4% of the solar energy spectrum and minority carrier rapid recombination due to the trap densities [7]. Fe_2O_3 narrow band gap (~2.1 eV) harvest visible light which consists 46% of the solar energy spectrum, stable in the aqueous solution, abundant, nontoxic and low cost [6]. However, the low electrical conductivity of hematite disrupts the continuous process of charge generation, transportation, collection and injection which resulting in the substantial loss of energy due to rapid electron-hole recombination [8,9]. Density functional theory (DFT) calculations suggest that the exciton binding energy (E_b) for Fe_2O_3 (41 meV) is larger than room thermal energy (25 meV) [9]. This literature follow-up emphasizes that no single material, whether TiO_2 or Fe_2O_3 meet the standards for efficient water oxidation. One potential approach towards the solution of intrinsic shortcoming with Fe_2O_3 and TiO_2 is to develop hetero-junction Ti-Fe-O (Fe_2TiO_5) pseudobrookite. Fe_2TiO_5 is an *n*-type

* Corresponding author.
E-mail address: alibahadur@chem.qau.edu.pk (A. Bahadur).
[1] These authors contributed equally.

http://dx.doi.org/10.1016/j.apcatb.2017.07.049
0926-3373/

semiconductor having band-gap energy of ca. 2.1 eV (depending on the synthesis method) with a wide absorption of visible light [10]. Fe_2TiO_5 is a low-cost, stable material. Moreover, the atomic and electronic structures match those of TiO_2 [11]. The conduction band (CB) of Fe_2TiO_5 (∼−0.7 eV) and TiO_2 (∼−0.5 eV) lies at nearly the same energy level which leads to a quick charge transfer under light illumination. Therefore, enhanced water oxidation performance can be obtained by developing a heterostructured between Fe_2TiO_5 and TiO_2.

Spatially separated yolk-shell structures with different components in the yolk and shell are desirable, [12–16] due to the promising stability and improved properties in the application of catalysis, energy storage, and drug delivery [17–20]. Thus, in this present work, pristine Fe_2TiO_5, pristine TiO_2, and Fe_2TiO_5-TiO_2 hetero-structure yolk-shell hollow spheres as FTYS-HS were constructed for photocatalytic water oxidation. The advantages of our designed FTYS-HS system are: 1) void hollow cavity ensures stability with low material density and enhances the surface area, hence more reactive sites available for the catalytic reaction. 2) The porous surface enables the solvent to access the reactive sites of the shells, hence, collect the minority carriers efficiently. 3) The forward and backward constructive interference at the surface and interface of yolk-shell enhance the incident photon lifetime in the material. The aim of this article was to provide the synthetic mechanism of FTYS-HS and investigate the water oxidation efficiencies related to a morphological aspect of designed structures. The article is organized as follows: Firstly, the synthetic mechanism is discussed in details with the help of structural characterizations of as-synthesized products. Then a detail discussion on the relative efficiency of each system determined for photocatalytic water oxidation.

2. Experimental

2.1. Materials

Hydrated ferric chloride ($FeCl_3{\cdot}6H_2O$, 99%), sucrose ($C_{12}H_{22}O_{11}$, 98.5%), Ethanol (C_2H_5OH, 99%), Titanium tetrachloride ($TiCl_4$, 98%), Silver Nitrate ($AgNO_3$, 98.5%), and distilled water all of analytical grade reagents were purchased from Beijing Chemical Reagent Factory and used without further purification.

2.2. Preparation of Fe_2TiO_5: TiO_2 hetero-structural yolk-shell hollow microspheres

2.2.1. Synthesis of the carbonaceous microsphere (CMS)

The synthesis of CMS were accomplished through polymerization emulsification process of sucrose hydrothermally as reported [21]. Briefly 130 g of sucrose dissolved in 250 mL deionized water and sealed in the Teflon autoclave for 2 h at 200 °C. After cooling down the reactor to room temperature, the brown suspension of CMS was collected, washed 4 times with water and ethanol. Final CMS were dried at 70 °C for 12 h and stored in desiccator for further use.

2.2.2. Synthesis of the Fe_2TiO_5-TiO_2 yolk-shell hollow spheres

In first step, 140 mL of pure $TiCl_4$ was poured into 200 mL of deionized water (DI) ice to attain strong hydrolysis subsequently formed 5 mol/L $TiCl_4$ aqueous solution. In second step, 0.5 g of the as-synthesized CMS was dispersed under sonication in 30 mL of the C_2H_5OH/H_2O (1:1) solution containing diluted 0.05 mol/L $TiCl_4$ and 0.03 mol/L $FeCl_3$. The resulting suspension was aged for 6 h under constant stirring at room temperature (RT), washed once with DI water followed by drying at 70 °C for 12 h. The dry sample was grinded, annealed in air from 25 °C to 500 °C at the heating speed of 1 °C min^{-1} and held at 500 °C for 1 h.

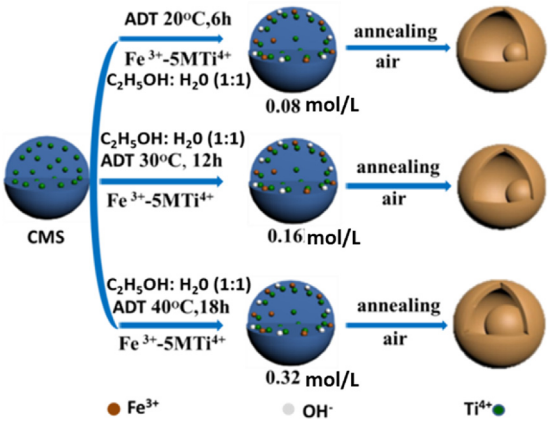

Fig. 1. The schematic illustration of the formation mechanism of Fe_2TiO_5-Yolk and TiO_2 in the shell.

2.3. Photochemical measurements

The rate of photochemical oxygen evolution from each catalyst was determined by irradiating 50 mg of catalyst, 50 mL of 0.01 mol/L $AgNO_3$ (aq.) at PH = 7 dispersed in 50 mL of water. Irradiations were performed in a quartz round-bottom flask with a 300 W Xe arc lamp (26.3 mW cm^2 at the flask λ = 250–380 nm) top irradiation, measured with a GaN photodetector. The airtight irradiation system connects a vacuum pump and a gas chromatograph (Varian 3800) with the sample flask to quantify the amount of gas evolved, using area counts of the peaks and the identity of the gas from the calibrated carrier times. Prior to irradiation, the flask was evacuated down to 5 Pa and purged with argon gas. This cycle was repeated until the chromatogram of the atmosphere above the solution indicated that the sample did not contain hydrogen, oxygen, or nitrogen.

2.4. Characterizations

Powder X-ray diffraction (XRD) patterns were recorded on a Panalytical X'Pert PRO MPD [Cu Kα radiation (λ = 1.5405 Å)], operating at 40 kV and 30 mA. Scanning electron microscopy (SEM) images were obtained to analyze morphology by using a JSM-6700 microscope operated at 5.0 kV equipped with an electron dispersive X-ray spectroscopy (EDX) system. Transmission electron microscopy (TEM), images were taken using an FEI Tecnai F20 instrument operated at an accelerating voltage of 200 kV. The thermogravimetric analysis-differential thermal analysis (TGA-DTA) data were collected using a DTA-60 (Shimadzu), annealed under air atmosphere at 1 °C min^{-1}. UV–vis-NIR spectrophotometer (Lambda 950, Perkin Elmer) equipped with an integrating sphere (150 mm diameter sphere covered with Spectralon as the reflecting material, Perkin Elmer). Emission spectra was carried out by a fluoromax-4 spectrofluorometer (Horiba Scientific Japan). Absorbance (A) measurements were obtained from measured reflectance (R, %) and transmission (T, %), using a wavelength range of 300–800 nm and a step of 5 nm, respectively.

3. Results and discussion

To obtain highly organized oxide, crystallization in the shells with control particle size and reproducible sacrificial carbonaceous microsphere (CMS) were employed as a hard template. Oxide spherical nanoshell self-assembled around the hollow cavity,

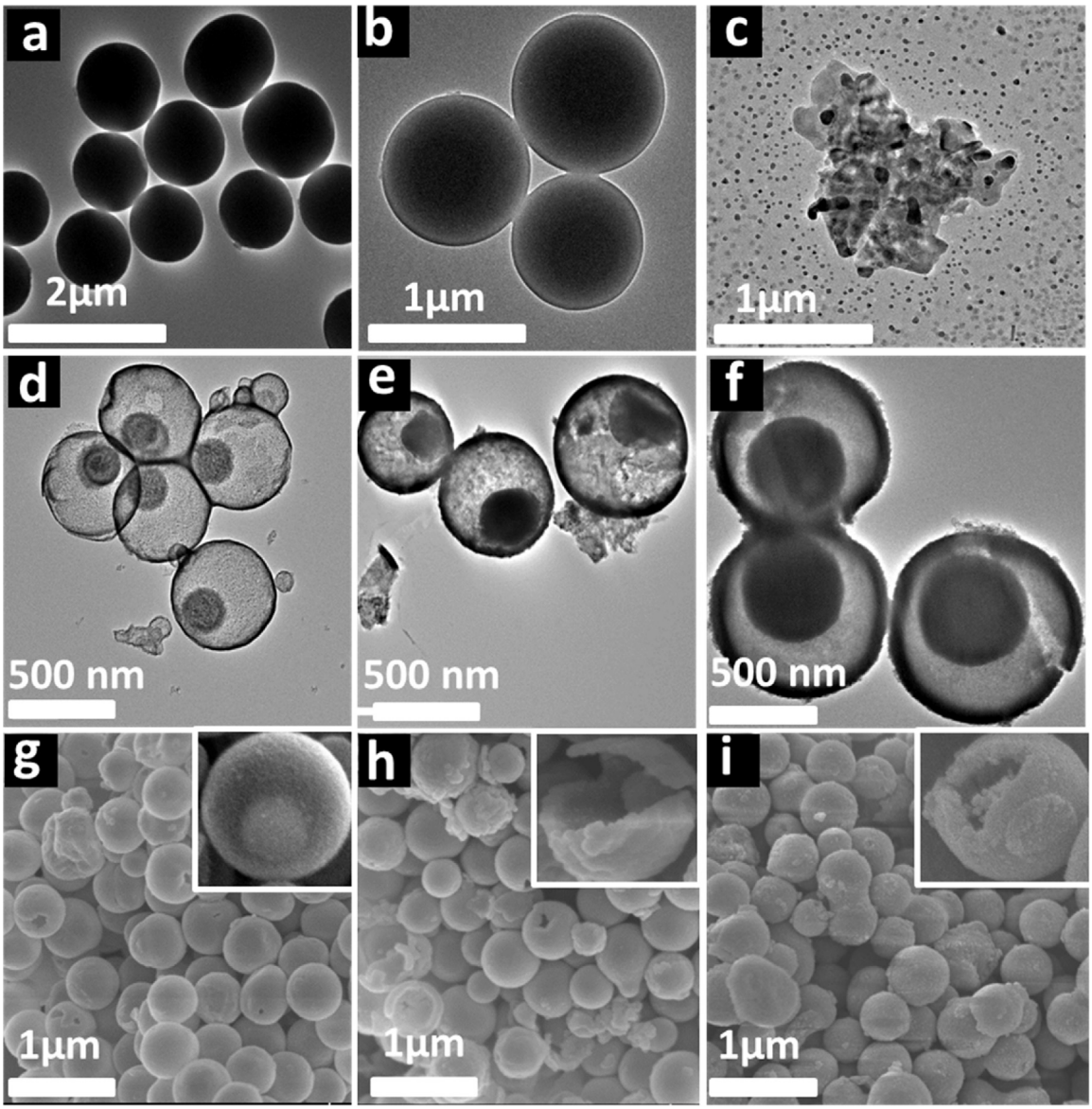

Fig. 2. TEM images of (a) carbonaceous microspheres (CMS) (b) CMS loaded with 0.08 mol/L (Fe^{3+}-Ti^{4+}) prior to annealing in the air, (c) oxidation of 0.08 mol/L (Fe^{3+}- Ti^{4+}) without using CMS as a template, (d and g) TEM and SEM of CMS loaded 0.08 mol/L (Fe^{3+}- Ti^{4+}) ions at 20 °C for 6 h (e and h) TEM and SEM of CMS loaded 0.16 mol/L (Fe^{3+}- Ti^{4+}) ions loaded on CMS for 12 h; thick, (f and i) TEM and SEM of CMS loaded 0.32 mol/L (Fe^{3+}- Ti^{4+}) ions loaded on CMS for 18 h; thicker yolk-shell of Fe_2TiO_5-TiO_2 hetero-structure hollow spheres respectively after annealing at 500 °C for 1 h.

produced by infusion of cations (Fe^{3+}-Ti^{4+}) through columbic interaction to the polyanions (OH^-: C=O) of CMS followed by calcining in the air. Parameters such as coordination ionic size (CIS), adsorption time (AT), adsorption temperature, (ADT), and precursor concentration (PC) were carefully optimized to obtain controlled desire structures (Fig. S1). The complete pictorial demonstration parameters of as-synthesized morphologies of CMS are shown in Fig. 1.

The transmission electron microscopy (TEM) analysis was performed to check the evolution of the synthesized functional CMS morphology (Fig. 2a). When polycations of (Fe^{3+}: Ti^{4+}) adsorbed at negatively charged CMS surface prior to the annealing in the air (Fig. 2b). In Fig. 2c, Fe^{3+}- Ti^{4+} turned into corresponding oxides without utilizing the template strategy.

To develop the spatially separated Fe_2TiO_5 in yolk and TiO_2 particles in the shell, the key step is to control the Ti coordination ionic radii (CIR). As shown in Fig. 3a, the formation of size prohibited complex anions $[Ti_nO_{4n}]^{4n-}$ was observed when 2 mol/L $TiCl_4$ (aq.) precursor was utilized [22]. The lack of recognition force between the precursor complex ions and carbonaceous polyanions inhibited the metal loading at the template surface. Metal oxide grows irrespective of the system upon annealing, which is a deviation of the feature characteristics of our template methodology, hence no shell formed. It is reported that smaller Ti coordination ion formed when 3 mol/L $TiCl_4$ solution used e.g., $[Ti(OH)_n(H_2O)_{6-n}]^{(4-n)+}$ (n = 2,3) and $[Ti_n(OH)_{2n}(H_2O)_{2n}]^{2n+}$ (n = 1) [23]. Cationic diffusion is proved when the polycondensates small enough to diffuse interstitial as well as the polycations recognized to the CMS polyanions [22]. Consequently, triple shell TiO_2 obtained (Fig. 3b). Further increasing the aqueous $TiCl_4$ concentration to 5 mol/L, $[Ti(OH)_nCl_{6-n}]^{2-}$ (n = 1,2,3) coordination anions are formed. Fig. 3a demonstrated that at 5 mol/L concentration, the polyanions adhered on the surface, the larger anion size and Columbic interactions, restricted the polyanions to deposit on the surface of CMS, however, dispersed TiO_2 particles observed in the core of the sphere. These findings directed us to load (ethanol: water 1:1) $FeCl_3{\cdot}6H_2O$ polycations precursor onto pre-adsorbed 5 mol/L $TiCl_4$ CMS through

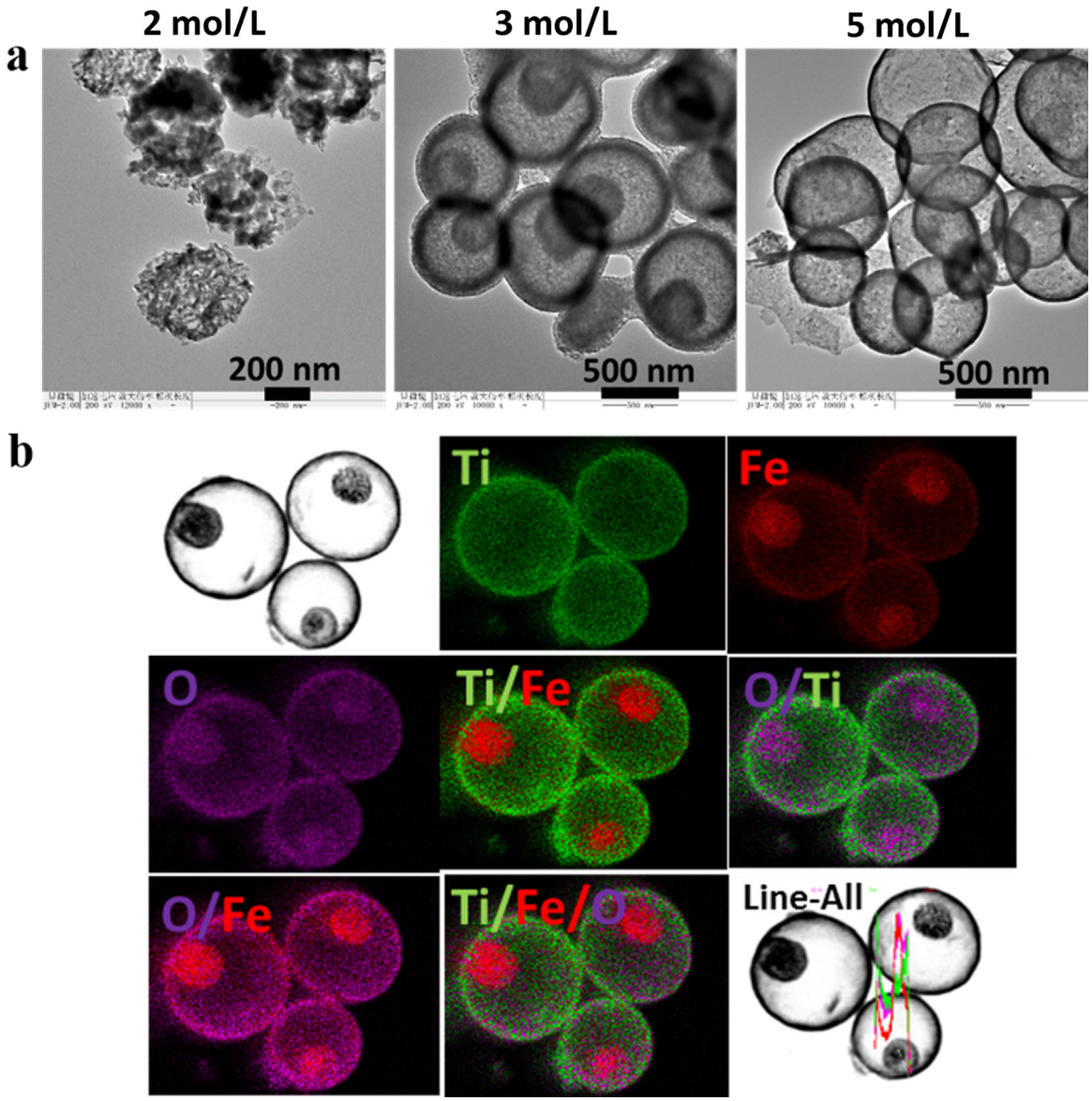

Fig. 3. (a) TEM images of 2, 3, 5 mol/L $TiCl_4$ immerse in CMS for 24 h at 40 °C followed by annealing in air for 1 h at 500 °C. (b) HAADF-Mapping of Fe_2TiO_5-TiO_2 Yolk-Shell morphology.

an interstitial mechanism. The wettability of aqueous solutions on hydrophobic or high-aspect surfaces was improved by the addition of ethanol [24]. It enhanced the radial diffusion of Fe^{3+} deep into the carbonaceous template. Furthermore, ethanol lowers the surface tension ($\sigma_{ethanol}$: 21.8 mN m^{-1} vs. σ_{water}: 72.0 mN m^{-1}) by disrupting hydrogen bonding and cohesive forces between water molecules hence enhances the wettability. This allows the Fe^{3+} ions to penetrate deep into the carbonaceous template [25]. When the total ionic concentration 0.08 M for (Fe^{3+}:Ti^{4+}) at 20 °C for 6 h were used, the penetration of Fe^{3+} polycations interstitially and agglomerates in the yolk of the template where it react with the Ti^{4+} ions through a solid state reaction, hence Fe_2TiO_5 in the yolk and thin TiO_2 in the shells obtained upon annealing (Fig. 2d). The mechanisms of radial diffusive transport into the CMS depends on the ionic charge, complex radial convection, and thermochemical effects during the mass loss of carbon in the combustion process [26]. Trivalent (Fe^{3+}) and tetravalent (Ti^{4+}) ion adopt a self-diffusion mechanism which operates on oxygen partial pressure and temperature [27]. Owing to the strong anisotropy of Fe over Ti (5 mol/L) both polycations dissolve spatially and diffuse interstitially [28]. Photon absorptions and charge separation process in the semiconductors are highly dependent on the light penetration depth with respect to the thickness of the material. Therefore we simultaneously applied Arrhenius equation [29] and Fick's first law [30] which stated that "at higher temperature rapid penetration and diffusion occur" and "a higher chemical diffusion achieve by using higher precursor concentration" respectively.

In consistent with theories, we increased the ADT from 20 °C to 30 °C, AT from 6 to 12 h and PC 0.08–0.16 mol/L, (Fig. 2e) controlled uniform thick FT-YSHS were obtained upon annealing in air. Further increasing the ADT; 30–40 °C, AT 6–18 h and PC 0.16–0.32 mol/L the thicker FTYS-HS were obtained (Fig. 2f). The corresponding SEM images of thin, thick and thicker FTYS-HS are shown in Fig. 2(g–I), respectively. We examined the HAADF-Mapping and thermogravimetric analysis (TGA) to get insightful information for FTYS-HS radial diffusion transport mechanism and radial combustion depth of CMS which lead to complete oxidation respectively (Figs. 3b and S2). The DTA curve at transition temperature (243 °C) suggested the TiO_2 shell formation as the carbon burn from the exterior of the template. Substantially, slower oxide formation was calculated

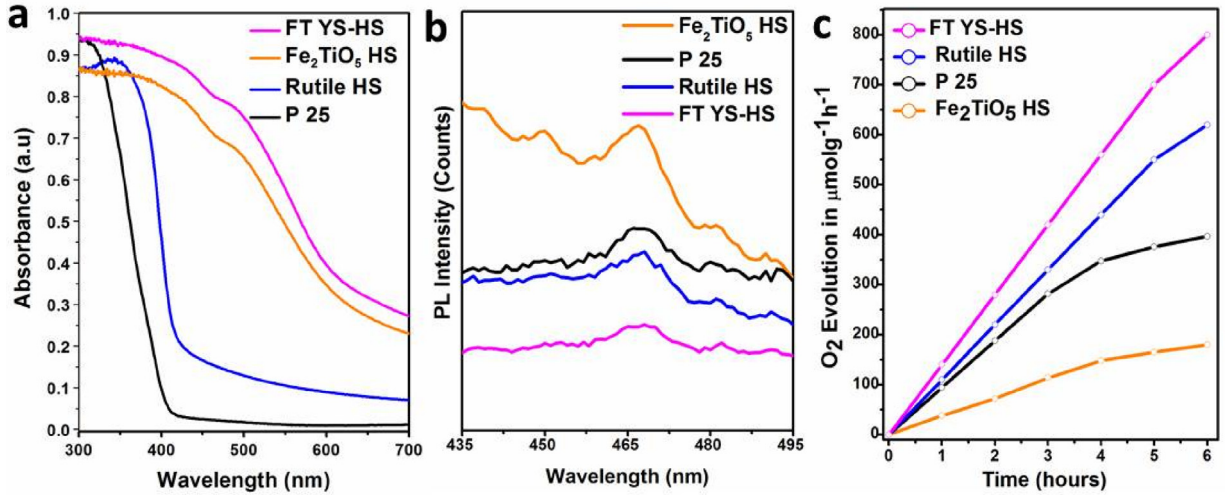

Fig. 4. (a) UV–visible spectra. (b) Photoluminescence (PL) and (c) Photocatalyst performance map of P25 commercial TiO_2, as synthesized rutile hollow spheres, Fe_2TiO_5 hollow spheres, and Fe_2TiO_5-TiO_2 hetero-structure hollow spheres respectively. Reaction conditions: 50 mg of sample dispersed in 50 mL of 0.01 mol/L $AgNO_3$ (aq.) at PH = 7, 300 W Xe lamp with full spectrum, top irradiation.

based on Cabrera-Mott and Fromhold-Cook models with respect to time [31]; it takes 600 years to form 4 nm thick oxide layer on iron film at room temperature [32]. Therefore by taking the advantage of exponential heating to accelerate the complete radial carbon combustion from exterior to the interior of template achieved at 400 °C. This allows the electron transport from the oxide shell layer to the adsorbed oxygen metal core substantially convert exposed metal core into oxide. The reaction front of Fe-O-Ti is determined by the relative diffusion of these species as well as temperature, shell thickness, and microstructure. Our experimental result suggested the inward diffusion flow of oxyanion is faster than outward Fe diffusion. However, after combustion of carbon in FTYS-HS at 400–500 °C was attributed to the crystallization of the thick concentrated metal oxide in the yolk. XRD pattern suggests the main peak composed of pure monophasic Fe_2TiO_5 (Fig. S3).

Ultra-violet Visible spectroscopy measurements are taken to find out the relation between the thickness versus absorbance on our design thin-thick and thicker FT-YSHS. It is clearly shown in Fig. S4a that all the designed morphologies exhibit good light absorbance. An increment in the thickness of spherical nanoshells and yolk by loading more metal precursors, the enhanced absorbance is promising as reported earlier by many groups [33]. However, the trade-off between material thickness and light absorption overrule in the performance context as suggested by Fig. S4c. PL data and O_2 evolution results indicated the excessive e^-/h^+ recombination due to the numerous grain boundaries in the thicker and thick FT-YSHS shells structures as compared to the thin FT-HS structure (Fig. S4b). These results help us to draw a conclusion that the optimal controlled shell and yolk thickness separates the photogenerated charges efficiently comparable thick and thicker counterpart structures.

Optical measurements of thin FT-YSHS are compared with Commercial TiO_2, as synthesised Fe_2TiO_5 and rutile hollow sphere to understand the difference in the catalyst performance with regard to morphology [34]. Fig. 4a shows the spectra of as-synthesised hollow spheres compared with commercial nanoparticles. Light absorption starts at 620 nm for Fe_2TiO_5 and FTYS-HS which gradually increases over the ultraviolet. The enhanced absorbance in the TiO_2 hollow spheres morphology over the TiO_2 nanoparticles attributed to the Omni-directional light trapping by the electronic hollow nanospheres shell [35]. In this system, a constructive interference of forwarding and backward propagation waves could prolong the photon lifetime in the hollow nanoshell sphere [36]. The absorbance spectrum of Fe_2TiO_5 and FTYS-HS suggested the geometry variation lead to enhance the resonant light trapping and harvests the maximum solar incident photons as possible between the near band edge of the absorber (λ_{0max} = 590 nm) for Fe_2TiO_5 and drop-off of the solar spectrum ($\lambda_0$min = 300 nm) for TiO_2.

Photoluminescence (PL) analysis was conducted to evaluate the separation efficiency of minority carriers in as-synthesized morphologies. Among all the FTYS-HS morphology showed the lowest peak signals which mean that the recombination rate of minority carriers is low (Fig. 4b). The photocatalytic activity was monitored for the TiO_2 rutile hollow sphere with the aid of single electron acceptor Ag^+. As displayed in Fig. 4c, the low evolved O_2 rate 110 μmol g^{-1} h^{-1} suggested the low mobility of holes (~0.27 s) in the rutile TiO_2 HS which does not match with the four hole chemistry rate; ~1 s require to release one molecule of oxygen [37]. In addition, power law stated that recombination of minority carriers is proportional to the excitation energy. Hence, by using excitation energy of an AM 1.5 G solar simulator potentially enhances the recombination of generated electrons and holes [38,39]. Less photocatalytic activity (26 μmol g^{-1} h^{-1}) was observed when pure Fe_2TiO_5 hollow sphere utilized under the same experimental conditions. This primarily denotes to the exciton binding energy E_b (meV), hole mass (m_h) for the TiO_2; (3 and 1.13), and for the Fe_2TiO_5; (18 and 1.59) respectively based on the density functional theory (DFT) calculations by S. Petit et.al [9]. Consequently, rapid recombination of minority carriers in the pure Fe_2TiO_5 HS over rutile TiO_2 HS observed as an account of activity difference. How to minimize the energy loss of nearly inactive pure Fe_2TiO_5 HS to recover its photocatalytic water oxidation properties? For this, Fe_2TiO_5 combined with TiO_2 in the heterostructure and evaluated the photocatalytic activity. The O_2 evolved at the rate of 148 μmol g^{-1} for the FTYS-HS in the first hour suggests that the Fe_2TiO_5-TiO_2 hetero-junction improves the charge separation process and limits the recombination rate (Table S1). The VB and CB edges are higher in Fe_2TiO_5 hollow spheres than in TiO_2 hollow spheres; this straddling gap in the heterostructure allows the charge transfer thermodynamically between the two systems [40]. Fig. 4c showed that O_2 produced in the first 5 h without any disruption. However, prolong reaction time course resulting in the excessive reduction of Ag^0 which blocks the incident light hence decline in the activity peak observed after 5.5 h.

We assumed that performance attributed to the geometry of our designed thin TiO_2 in the shell and Fe_2TiO_5 yolk which enable mul-

tiple reflections. The propagating incidents photons entered from all sides of the spherical structure, hence a constructive interference of forward and backward photons improved the light harvesting in the hollow spheres. The hetero-junction of thin TiO_2 shell and Fe_2TiO_5 yolk efficiently separated the minority carriers. The hollow cavity and wide distribution of meso, micro and macrospores allow the solvent to adsorb on the active sites, hence reduce the diffusion length of minority carriers (Fig. S5). Combine the optimization of Fe_2TiO_5-TiO_2 heterostructure in the yolk-shell hollow spheres, a good trade-off between light absorption to charge generation, transfer and charge collection were achieved. Currently, we are extending this simple, facile methodology to synthesize mixed metal oxynitride hollow nanoshells heterostructures with control porosity for the simultaneous solar is driven oxidation and reduction reactions.

4. Conclusions

A simple and facile sacrificial hard template strategy was utilized to synthesized spatially separated Pseudobrookite (Fe_2TiO_5-TiO_2) yolk-shell hollow spheres. Combined and controlled Fe_2TiO_5 phase as the yolk and TiO_2 as the shells of hollow spheres structure was obtained. Different concentrations (2–5 mol/L) of $TiCl_4$ precursor in water were soaked into the carbonaceous template for 24 h adsorption time. To facilitate the Fe^{3+} ions radial penetration into the hydrophobic core of carbonaceous template, we optimized the ethanol to water ratio (1:1). The Fe_2TiO_5-TiO_2 yolk-shell hollow spheres exhibit the high oxygen evolution reaction (OER) rate up to 148 $\mu mol\, g^{-1}\, h^{-1}$ under UV–vis light. This attributed to the better light harvesting properties due to its geometry; charge separation by a thin shell, a void cavity to assess reaction solvent assessable to reactive sites of structure and the hetero-junction of Fe-O-Ti. These findings suggest that our design multi-shelled Fe_2TiO_5-TiO_2 yolk-shell hollow spheres are beneficial for the photocatalytic water oxidation.

Acknowledgements

This project was kindly supported by the Chinese Academy of Sciences (CAS) and the Academy of Sciences for the Developing World (TWAS) President's Fellowship Programme, CAS-TWAS Postgraduate Fellowship.

Appendix A. Supplementary data

Supplementary data associated with this article can be found, in the online version, at http://dx.doi.org/10.1016/j.apcatb.2017.07.049.

References

[1] J. Luo, J.-H. Im, M.T. Mayer, M. Schreier, M.K. Nazeeruddin, N.-G. Park, S.D. Tilley, H.J. Fan, M. Grätzel, Science 345 (2014) 1593–1596.
[2] L. Liu, Y.Y. Peter, X. Chen, S.S. Mao, D. Shen, Phys. Rev. Lett. 111 (2013) 065505.
[3] K. Sivula, J. Phys. Chem. Lett 4 (2013) 1624–1633.
[4] T.W. Hamann, Dalton Trans. 41 (2012) 7830–7834.
[5] A.J. Cowan, J. Tang, W. Leng, J.R. Durrant, D.R. Klug, J. Phys. Chem. C 114 (2010) 4208–4214.
[6] K. Sivula, F. Le Formal, M. Grätzel, ChemSusChem 4 (2011) 432–449.
[7] M. Ni, M.K. Leung, D.Y. Leung, K. Sumathy, Renew. Sustain. Energy Rev. 11 (2007) 401–425.
[8] H. Dotan, O. Kfir, E. Sharlin, O. Blank, M. Gross, I. Dumchin, G. Ankonina, A. Rothschild, Nat. Mater. 12 (2013) 158–164.
[9] S. Petit, S.T. Melissen, L. Duclaux, M.T. Sougrati, T. Le Bahers, P. Sautet, D. Dambournet, O. Borkiewicz, C. Laberty-Robert, O. Durupthy, J. Phys. Chem. C 120 (2016) 24521–24532.
[10] J. Deng, X. Lv, J. Liu, H. Zhang, K. Nie, C. Hong, J. Wang, X. Sun, J. Zhong, S.-T. Lee, ACS nano 9 (2015) 5348–5356.
[11] P.S. Bassi, S.Y. Chiam, J. Barber, L.H. Wong, ACS Appl. Mater. Interfaces 6 (2014) 22490–22495.
[12] J. Liu, S.Z. Qiao, S. Budi Hartono, G.Q.M. Lu, Angewandte Chemie 122 (2010) 5101–5105.
[13] H. Li, Z. Bian, J. Zhu, D. Zhang, G. Li, Y. Huo, H. Li, Y. Lu, J. Am. Chem. Soc. 129 (2007) 8406–8407.
[14] X.W.D. Lou, L.A. Archer, Z. Yang, Adv. Mater. 20 (2008) 3987–4019.
[15] K. Kamata, Y. Lu, Y. Xia, J. Am. Chem. Soc. 125 (2003) 2384–2385.
[16] X. Lai, J. Li, B.A. Korgel, Z. Dong, Z. Li, F. Su, J. Du, D. Wang, Angewandte Chemie 123 (2011) 2790–2793.
[17] J. Lee, J.C. Park, H. Song, Adv. Mater. 20 (2008) 1523–1528.
[18] W. Li, Y. Deng, Z. Wu, X. Qian, J. Yang, Y. Wang, D. Gu, F. Zhang, B. Tu, D. Zhao, J. Am. Chem. Soc. 133 (2011) 15830–15833.
[19] Z. Dong, X. Lai, J.E. Halpert, N. Yang, L. Yi, J. Zhai, D. Wang, Z. Tang, L. Jiang, Adv. Mater. 24 (2012) 1046–1049.
[20] X. Lai, J.E. Halpert, D. Wang, Energy Environ. Sci. 5 (2012) 5604–5618.
[21] Y. Lu, Y. Zhao, L. Yu, L. Dong, C. Shi, M.J. Hu, Y.J. Xu, L.P. Wen, S.H. Yu, Adv. Mater. 22 (2010) 1407–1411.
[22] H. Ren, R. Yu, J. Wang, Q. Jin, M. Yang, D. Mao, D. Kisailus, H. Zhao, D. Wang, Nano Lett. 14 (2014) 6679–6684.
[23] V. Hildenbrand, H. Fuess, G. Pfaff, P. Reynders, Zeitschrift für Physikalische Chemie 194 (1996) 139–150.
[24] Z. Yuan, H. Chen, J. Tang, X. Chen, D. Zhao, Z. Wang, Surf. Coat. Technol. 201 (2007) 7138–7142.
[25] S. Xu, C.M. Hessel, H. Ren, R. Yu, Q. Jin, M. Yang, H. Zhao, D. Wang, Energy & Environmental Science 7 (2014) 632–637.
[26] P.A. Libby, T.R. Blake, Combust. Flame 36 (1979) 139–169.
[27] J. Sasaki, N. Peterson, K. Hoshino, J. Phys. Chem. Solids 46 (1985) 1267–1283.
[28] J. Steele, E. McCartney, Nature 222 (1969) (79-79).
[29] K.J. Laidler, J. Chem. Educ. 61 (1984) 494.
[30] D. Straub, R. Graue, F. Heitmeir, P. Nebendahl, T.K. Wurst, Propellants, Explosives Pyrotechnics 12 (1987) 105–112.
[31] N. Cabrera, N. Mott, Rep. Prog. Phys. 12 (1949) 163.
[32] C.M. Wang, D.R. Baer, L.E. Thomas, J.E. Amonette, J. Antony, Y. Qiang, G. Duscher, J. Appl. Phys. 98 (2005) 094308.
[33] M. Rioult, H.l.n. Magnan, D. Stanescu, A. Barbier, J. Phys. Chem. C 118 (2014) 3007–3014.
[34] J. Tauc, R. Grigorovici, A. Vancu, Physica status solidi (b) 15 (1966) 627–637.
[35] Y. Fink, J.N. Winn, S. Fan, C. Chen, J. Michel, J.D. Joannopoulos, E.L. Thomas, Science 282 (1998) 1679–1682.
[36] L. Zeng, P. Bermel, Y. Yi, B. Alamariu, K. Broderick, J. Liu, C. Hong, X. Duan, J. Joannopoulos, L. Kimerling, Appl. Phys. Lett. 93 (2008) 221105.
[37] J. Tang, J.R. Durrant, D.R. Klug, J. Am. Chem. Soc. 130 (2008) 13885–13891.
[38] A. Barzykin, M. Tachiya, J. Phys. Chem. B 106 (2002) 4356–4363.
[39] J. Nelson, S.A. Haque, D.R. Klug, J.R. Durrant, Phys. Rev. B 63 (2001) 205321.
[40] Q. Liu, J. He, T. Yao, Z. Sun, W. Cheng, S. He, Y. Xie, Y. Peng, H. Cheng, Y. Sun, Nat. Commun. 5 (2014).